JOURNAL DE PHYSIQUE Colloque C10, supplément au n°12, Tome 41, décembre 1980, page C10-269

THE SPIN SPECTROMETER AT THE HOLIFIELD HEAVY-ION RESEARCH FACILITY AND SOME PLANNED EXPERIMENTS

D.G. Sarantites, M. Jääskeläinen, J.T. Hood, R. Woodward, J.H. Barker*, D.C. Hensley**, M.L. Halbert** and Y.D. Chan**.

*Department of Chemistry, Washington University, St. Louis, MO 63130, U.S.A.
**Department of Physics, St. Louis University, St. Louis, MO 63103, U.S.A.
**Oak Ridge National Laboratory, Oak Ridge, Tennessee 67830, U.S.A.

Abstract.- The 4π multidetector γ-ray spectrometer at the Holifield Heavy-ion Research Facility (HHIRF) is described in some detail. The following important features of this spectrometer are discussed: (a) the geometric arrangement, (b) the actual performance of the individual detector elements, (c) the associated electronics and data acquisition system , and (d) the response of the system to input γ-cascades including the effect of crystal-to-crystal scattering and the response to neutrons. The first few experiments to be performed are briefly described.

1. INTRODUCTION

A new type of γ-ray spectrometer for investigations of the mechanisms of heavy-ion induced reactions and of the structure of nuclei at high angular momentum was constructed at Washington University and installed at the HHIRF at the Oak Ridge National Laboratory. It consists of 72 NaI separate detector elements closely packed in a 4π arrangement. This system records on an event-by-event basis for each detector that fires its identifying bit, the associated pulse height, the time of triggering, and the pulse width. From these data the following information can be obtained on an event-by-event basis: (a) the coincidence fold k and thus the associated γ-ray multiplicity M_γ, (b) the associated total pluse height H and thus the total γ-ray energy E^*, (c) the associated pulse height spectrum $\{h_i\}_{i=1,\ldots,k}$ and thus the energy spectrum associated with a given (E^*,M_γ) d) the identification of pulses due to neutrons and thus the neutron multiplicity, (e) the identification of coincidence summing due to neutrons and γ-rays, thus providing clean response to γ-rays, (f) the time relationships of the various γ-rays in each cascade, and (g) the angular correlations of the γ-rays in each cascade. Additional valuable information can be obtained from second and higher order correlations, e.g, E_γ-E_γ, H-k-E_γ, H-k-E_γ-E_γ, E_γ-E_γ-E_γ, H-k-t, H-k-t-E_γ, etc.

For a given γ-ray cascade from fusion-like heavy-ion reactions a linear relationship exists between M_γ and the initial angular momentum J from where the γ-cascade starts. Therefore, the event-by-event recording of the fold k and thus of M_γ permits one to associate with each event a value of the transferred angular momentum J. This is the basis for choosing the name Spin Spectrometer for this instrument.

It should be understood that in most of the experiments with the Spin Spectrometer one or more additional selective detectors can be used. These include Ge(Li) counters, ΔExE heavy-ion or light

particle telescopes, neutron time-of-flight detectors, etc.

The theory and general characteristics of 4π γ-ray multidetector systems for investigations of high-spin phenomena have been presented in considerable detail in Ref. 1. Therefore only the characteristics of the spectrometer at the HHIRF will be discussed here.

2. GEOMETRY OF THE SPECTROMETER

The 72 NaI detector elements are closely packed as a hollow sphere with an inner diameter of 35.6 cm and a shell thickness of 17.8 cm. Each detector is a tapered prism that can be removed radially from the sphere. The cross section of twelve of the detectors is a regular pentagon. Each pentagonal detector is surrounded by five hexagonal detectors. All detectors subtend the same solid angle. A cluster of 10 detectors is seen in Fig. 1. The shape of the polygons in the inner

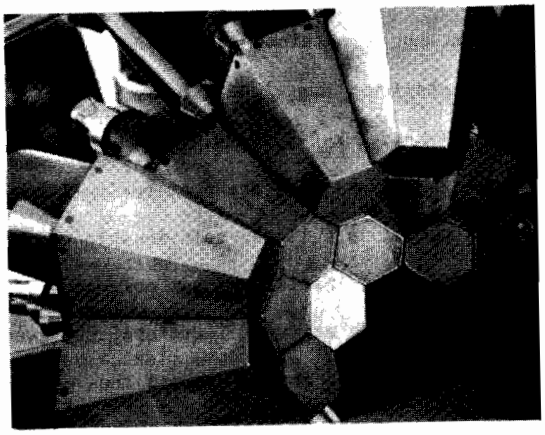

Fig. 1. A cluster of 10 detectors showing the shape of the detectors and their close packing.

sphere is clearly seen. In the complete polyhedron there are 120 three-fold vertices. The spherical shell is held together by 120 clamps each bolted to three adjacent detectors. The supporting frame is a split regular dodecahedron with edges consisting of 25.4 mm diameter, anodized aluminum rods. Eight radial struts (25.4 mm diameter) anodized aluminum) connect each half of the shell to each half of the frame. In turn each half of the frame rests on a 25 mm thick 90 cm x 180 cm anodized plate that can travel on tracks a distance of 60 cm perpendicular to the beam direction to give access to the enclosed scattering chamber. The angle between the axes of adjacent detectors is 25°, and the total effective solid angle is 96.5% of 4π. The present spherical scattering chamber has an inner diameter of 32 cm and provides one port for the target holder, three ports for Ge(Li) detectors, and mounts for particle detectors between 5° and 175° to the beam direction in one or two planes. Fig. 2 shows the scattering chamber

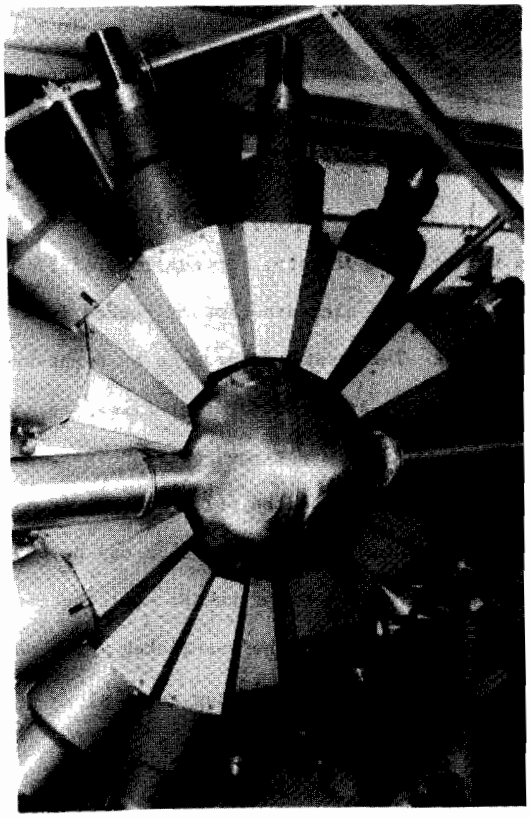

Fig. 2. Closeup view of the scattering chamber with one half of the spectrometer in its nearest normal position.

surrounded by one of the halves of the spectrometer. Fig. 3 shows the complete spectrometer

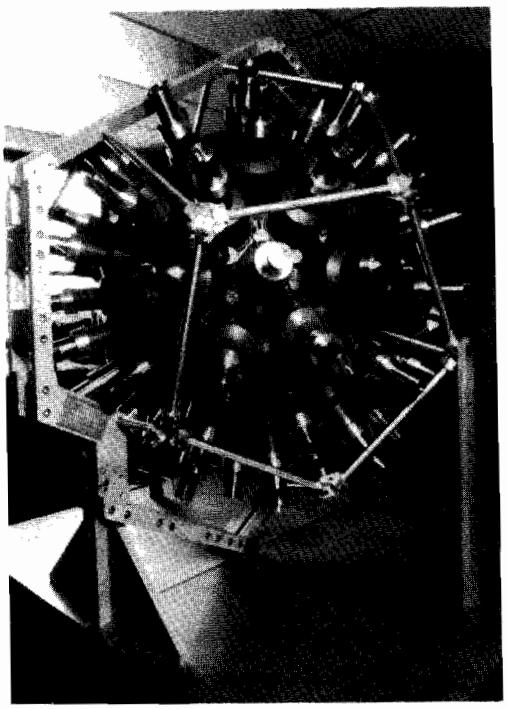

Fig. 3. Complete view of the Spin Spectrometer without the cables and the beam line.

without the cables and the beam line, and Fig. 4

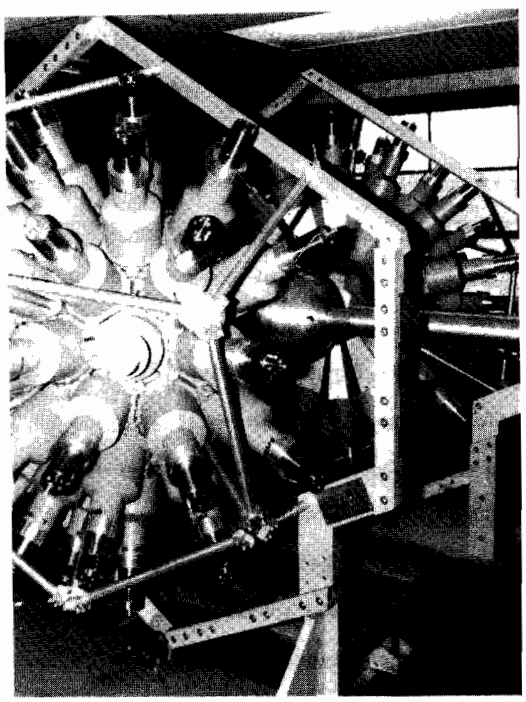

Fig. 4. Closeup view of the spectrometer open to give access to the enclosed scattering chamber.

shows the complete spectrometer with the two halves separated to a distance of 120 cm with the scattering chamber in mid position.

3. PREFORMANCE OF THE DETECTORS

Each detector consists of polyscin material [2] integrally coupled via a curved glass window to an RCA 4522 photomultiplier tube. Presently, resistive voltage dividers are employed with a chain current of ∿1.8 mA at 2,000 V. The average operating voltage for optimal overall performance is -1900 V.

The average timing resolution is 2.1 ns FWHM and 4.7 ns FWTM when measured with a constant fraction timing discriminator (CFTD) with the threshold set at 80 keV using a ^{60}Co source. The detectors with the best timing characteristics were placed at the forward angles. This is shown in Fig. 5

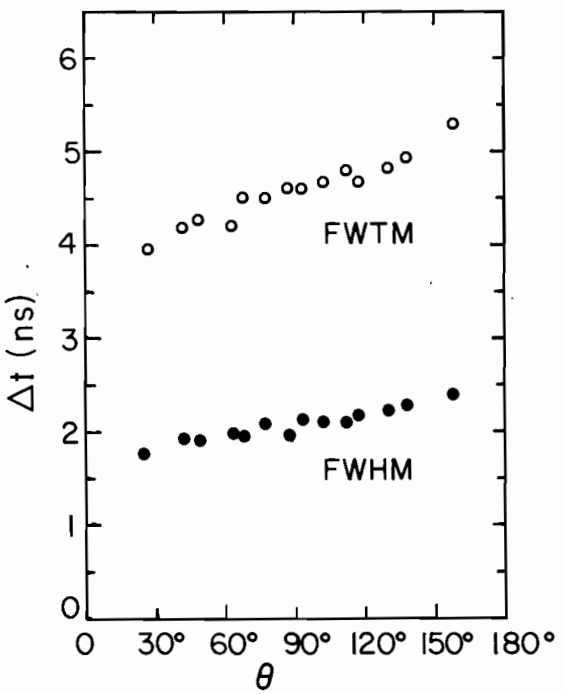

Fig. 5. Average timing resolution over 5 detectors that form an angle θ with respect to the beam. The detectors with the best timing resolution were placed at forward angles.

where the average timing over five equivalent detectors is plotted vs. the angle with respect to the beam.

The average energy resolution $\Delta E_\gamma/E_\gamma$ is 8.6%

and 6.3% for 662 keV and 1332 keV, respectively. The average energy resolution for each group of five equivalent detectors in the spectrometer is shown in Fig. 6 as a function of the angle θ for the 662 keV and 1332 keV lines. For counting rates

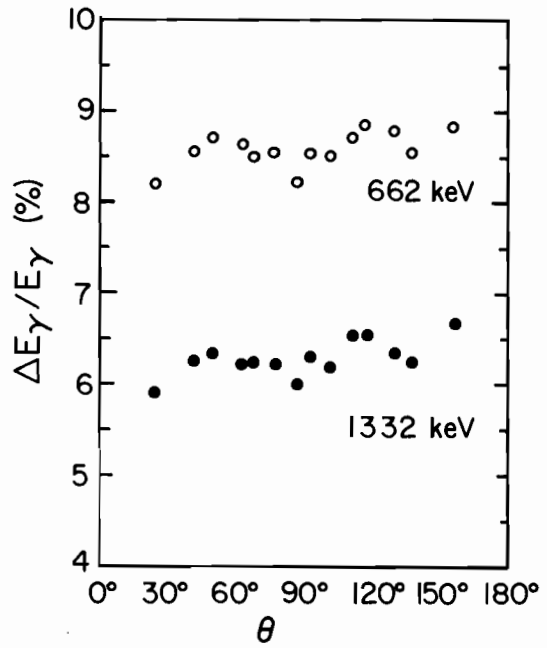

Fig. 6. Average energy resolution for each group of five equivalent detectors forming an angle θ to the beam.

up to ∿50,000 c/s less than 0.1% loss in resolution at 662 keV was observed. Increasing the counting rate to 75,000 c/s, however, resulted in decrease in energy resolution from 8.5% to 9.8%.

The average pulse height variation (uniformity) $\Delta E_\gamma/E_\gamma$ along the detector length is 3% when measured with a collimated ^{137}Cs source. The detector response was found to be linear for the range of 0-2.5 MeV employed in the tests. Measurements of the gain stability over a period of several weeks did not show any significant shift. For the temperature range 18°-24° C the gain at 662 keV was found to decrease by 0.3% per °C. This shift was due to the combined effect of the detector, phototube, and voltage supply.

The gain shift with counting rate of a typical detector is shown in Fig. 7 for several operating voltages. For the lower voltages there is little

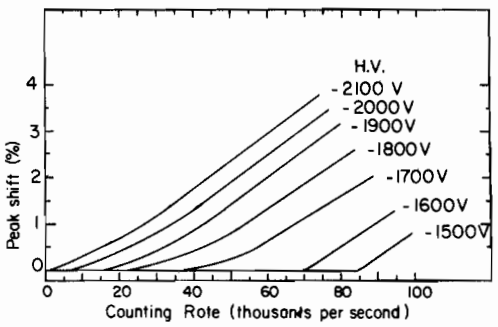

Fig. 7. Percent peak position shift for 1332 keV with counting rate measured at the indicated operating voltages.

or no shift up to ∿50,000 c/s and for higher voltages a linear shift of ∿0.7% per 10,000 c/s is observed. With the present voltage dividers, the limit of 1.0% in gain shift for 1332 keV is found to be in the range 30,000-100,000 c/s when the highest acceptable voltages are used.

4. ELECTRONICS AND DATA ACQUISITION SYSTEM

A schematic diagram of the electronics arrangement is shown in Fig. 8. The photomultiplier anode signal is first amplified by a fast x10 preamplifier. One of the pre-amplifier outputs is shaped to an approximately triangular shape (FWHM of ∿100 ns, FWTM of ∿200 ns), delayed by 300 ns, and then fed into a charge integrating ADC. The second output is used to trigger a front edge CFTD and a second rear edge CFTD, which is sensitive to a second pulse arriving in the range <8 ns to 240 ns after the first pulse. The time difference between the two discriminators produces a fixed amplitude pulse the width of which

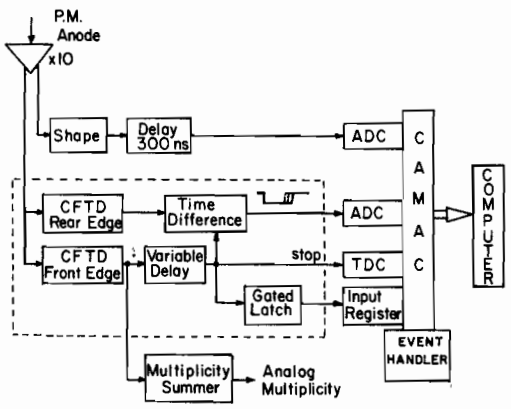

Fig. 8. Schematic diagram of the electronics (see text).

is a measure of the time difference between the two pulses arriving at the same detector. This time difference is digitized via a charge integrating ADC. After an adjustable delay (0-150 ns), the front edge CFTD output is used to stop a time-to-digital converter (TDC) and set the corresponding bit in a strobed gated latch. A 72-channel multiplicity summer, capable of providing the coincidence fold as a fast analog signal, is also generated. In addition to the 72 bits for NaI, 16 bits for other associated detectors can be set in the gated latch. The two sets of 72 ADC's and one set of TDC's are coupled to a CAMAC system.

The information management and data acquisition occurs via the EVENT HANDLER [3], a programmable CAMAC based controller, which is a device to select events that meet the user's criteria, place them in a suitable format, and transmit them to the on-line computer. The computer program in turn may apply further selection, buffering and formating before the events are recorded permanently. It may also provide for on-line sampling of the data. Data from other selective detectors may be processed by additional CAMAC modules and interface via the same EVENT HANDLER. The time required for digitizing the signals and transmitting them to the computer limits the data acquisition to ∿5,000 events/s.

The operating characteristics of all NaI detectors are stored in a disk file. The setup and data acquisition programs have access to this file to obtain whatever information they require on the detector parameters. Changes may be inserted into this file by the setup programs. Printouts of the disk file are made on request or when changes are completed. Major discrepancies between the current file and earlier ones are automatically brought to the attention of the user as a warning of possible detector malfunction.

The phototube high voltages are furnished by computer controlled power supplies. The high voltages are initially set by reference to the disk file.

All detectors are operated with the same pulse-height gain and the same time scale in order to minimize the event processing time. The uniform-gain requirement is met by automatic adjustment of the phototube voltage on the basis of spectra from a γ-ray source. The gain-setting program cycles through all the detectors in succession, accumulating data for a few seconds per detector. A peak-search routine then determines the locations of the selected lines and the high voltage is adjusted, if required, to give the standard gain.

The time scale is made uniform for each detector by manual adjustment of each TDC unit. The time scales and timing resolution are checked automatically by another program using data from a source with coincident γ-rays. At present the CFTD threshold adjustments are manual, but provision for computer control has been made.

5. THE RESPONSE OF THE SYSTEM

In general, a measurement of high multiplicity

events consits of recording a collection of pulse-heights $\{h_i\}_{i=1,\ldots,k}$ when the input spectrum is $\{E_i\}_{i=1,\ldots,M_\gamma}$. The maximum information is contained in the probability $P_N(k,h_1\ldots h_N;E_1\ldots E_{M_\gamma})$ that detector 1 records pulse-height h_1, etc., when only k of $h_1,\ldots,h_N$ are above threshold. Expressions for this and other related probabilities have been derived in Ref. [1]. This general probability can be constructed from calibrations. It is the reverse problem, however, that is of considerable interest. This involves the best characterization of $\{E_i\}_{i=1,\ldots,M}$ from a collection of measurements through the connection given by $P_N(k,h_1\ldots h_N;E_1\ldots E_{M_\gamma})$.

Restricting ourselves here to fusion-like reactions we note that nuclei can only be prepared with a population of the entry states [4] characteristic of the reaction system employed. Clearly, we would like to characterize the decay modes of each entry state (E^*,J). The decay $(E^*,J) \rightarrow (0,J_{g.s})$ to the ground state results in a γ-ray spectrum $n(E)dE = \sum_i n(E_i)dE$, where the sum is over all the possible decay paths. The important characteristic of these pathways is that they have a common total energy E^*, but different decay spectra that produce in turn a distribution in γ-ray multiplicity. Let this distribution be represented by $P_N(E^*J \rightarrow E^*M_\gamma)$. This mapping is shown schematically in Figs. 9a and b. The various lines in Fig. 9a represent different pathways each with a given M_γ value and an associated decay spectrum. Upon measurement, each point in the (E^*,M_γ) space maps into a domain in (H,k) (Fig. 9c) represented by the distribution $P_N(E^*M_\gamma \rightarrow Hk)$, where the total pulse height is $H = \sum_i h_i$. The latter distribution represents one of the possible response functions of the apparatus, and it can be well characterized by its first few moments [1]. Calculations based

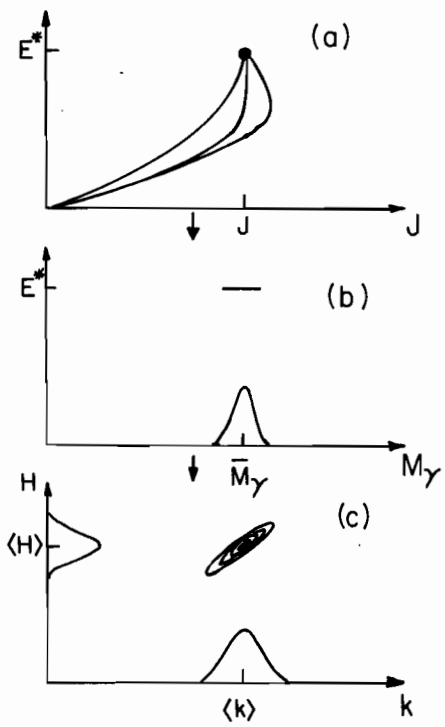

Fig. 9. (a) Schematic representation of the pathways for the decay $(E^*J) \rightarrow (0,J_{g.s})$. (b) Representation of the decays shown in (a) into the (E^*,M_γ) space. (c) Response of the spectrometer to the distribution from (b). The projections on the M_γ or the H and k axes are shown schematically.

on initial estimates of detection efficiencies for this spectrometer show that for given E^* the mean $\langle H\rangle$ is a weak function of M_γ and that for given M_γ the mean $\langle H\rangle$ is essentially proportional to E^*. Similarly, for given E^* we find [see also Ref. 1] that $\langle k\rangle$ is essentially a linear function of M_γ and that for given M_γ the values of $\langle k\rangle$ is insensitive to changes in E^*.

Analytic expressions for the response $P_N(E^*M_\gamma \rightarrow Hk)$ and for its moments have been given in Ref. 1 and comparisons for spectrometers with different numbers of detectors have been made. The main characteristics of the response $P_N(E^*M_\gamma \rightarrow Hk)$ are shown in Fig. 10, where the response was evaluated via eq. 49 of Ref. 1, for $E^* = 30$ MeV, and $M_\gamma = 30$. In general, this bivariate

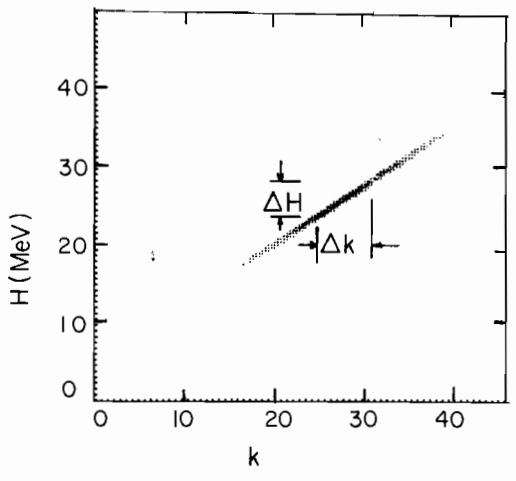

Fig. 10. Density plot of the response $P_N(E^*M_\gamma \rightarrow Hk)$ using the expression 49 in Ref. 1 for $E^* = 30$ MeV and $M_\gamma = 30$. The quantities ΔH and Δk indicate the FWHM values of the projections on the H and k axes, respectively.

distribution will be narrower than that shown schematically in Fig. 9c, because the latter incorporates the width of the M_γ distribution from Fig. 9b. However, we note that in the approximation of eq. 49 in Ref. 1 the higher order correlation terms such as $\langle H^2k\rangle$, $\langle Hk^2\rangle$, etc., have been ignored. This may cause the width in k to vary for different values of H, although the overall widths σ_H and σ_k for the projections remain unaffected.

In many experiments the population distributions Q(H,k) will be determined. The desired population $R(E^*,M_\gamma)$ is then obtained as a solution to the equations $\sum_{E^*,M} R(E^*M_\gamma) \cdot P_N(E^*M_\gamma \rightarrow Hk) = Q(H,k)$. We have employed iterative procedures for solving this system of equations.

The one-to-one correspondence shown in Figs. 9a,b,c between $(E^*,J) \leftrightarrow (E^*,\bar{M}_\gamma) \leftrightarrow (\langle H\rangle, \langle k\rangle)$ is an important feature of this spectrometer. It permits for each experiment selection of a class of events associated with a pair of values (H,k) that corresponds to a region in (E^*,M_γ) and thus in (E^*,J) space. The selected distribution in (E^*,J) has a similar shape with that shown in Fig. 9c. This particular type of selection, although not unique, is expected to be used most commonly due to its simplicity. The ability of the Spin Spectrometer to select events associated with a rather small region of the available (E^*,J) space opens many new possibilities for study of high spin phenomena both from the point of view of reaction mechanisms and of nuclear structure in a large number of experiments as outlined briefly in the introduction.

The actual response function $P_N(E^*M_\gamma \rightarrow Hk)$ of the spectrometer can be constructed from suitable calibrations with radioactive sources. There are, however, some important physical effects that determine in general the response of the spectrometer to a given input via the detection statistics. These were discussed in detail in Ref. 1. Briefly, these are: (a) Incomplete detection due to the fact that the total detection efficiency Ω_T is less than 1. (b) Crystal-to-crystal scattering due to lack of shielding between detector elements which is required to minimize the effect of (a) above. This causes more than one detector to fire due to a single γ-ray. (c) Coincidence summing that originates from the finite probability that more than one γ-ray from a given event may interact with the same detector and result in a single response. (d) Indistinguishable pulses that arise from the fact that neutrons or high energy protons may trigger some detector elements. This is particularly true in the forward detectors.

The effect of incomplete detection can be minimized by optimal packing of the detectors and by use of thick spectrometer shells. The detailed calibration for triggering and energy deposition of our spectrometer is now in progress. The crystal-to-crystal scattering effects the relation

of the multiplicity to the fold k and the multiplicity resolution [1]. As part of the procedure to determine these relationships more accurately we have measured the crystal-to-crystal scattering for the entire spectrometer using monoenergetic sources of ^{137}Cs (662 keV) and ^{54}Mn (834 keV).

Let Ω'_i be the triggering efficiency for the i^{th} detector for single response and Ω''_{ij} the triggering efficiency for double response between the ij detector pair. We can define the total single and double triggering efficiencies by $\Omega' = \sum_i \Omega'_i$ and $\Omega'' = \sum_{ij, i\neq j} \Omega''_{ij}$. If the i^{th} detector is selected to be a pentagonal one, then there are 5 equivalent j detectors that form the same angle θ with respect to the i^{th} detector. The scattering correlation function is then given by

$$F''(\theta) = \sum_{ij, i\neq j} \Omega''_{ij}/(\Omega' + \Omega'') ,$$

where for a given detector i the sum over j is limited to the five detectors with the same θ. The total double scattering is then $F'' = \sum_\theta F''(\theta)$. Fig. 11 shows the scattering correlation function $F''(\theta)$ measured for 662 keV (open circles) and 834 keV (closed circles). The total scattering factors F'' are 0.19 and 0.24 for 662 and 834 keV, respectively. It is seen that for $\theta \gtrsim 60°$ the scattering is essentially constant.

The effect of response to neutrons on the first two moments of the response $P_N(E^*M_\gamma \rightarrow Hk)$ was discussed in considerable detail in Ref. 1. The large cross section for inelastic scattering of neutrons on iodine when combined with the large thickness of NaI may cause significant interfernce due to response to neutrons. Thus pulses due to neutrons must be identified by their time-of-flight (TOF). Fig. 12 gives the calculated TOF, Δt, as a function of neutron energy E_n for three distances of 18, 27 and 36 cm corresponding to the front, middle, and back of each NaI detector in this spectrometer.

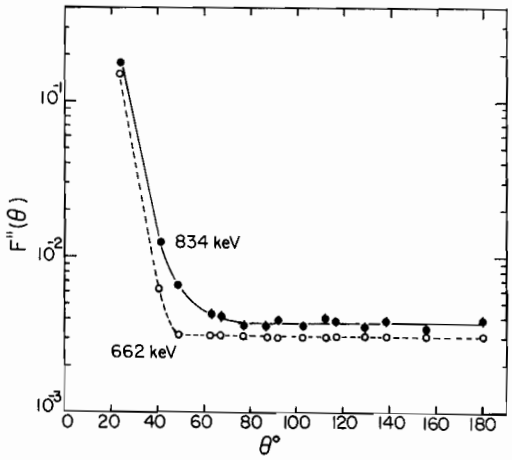

Fig. 11. Scattering correlation function F''(θ) for groups of five equivalent detectors. Results for two incident γ-ray energies are given.

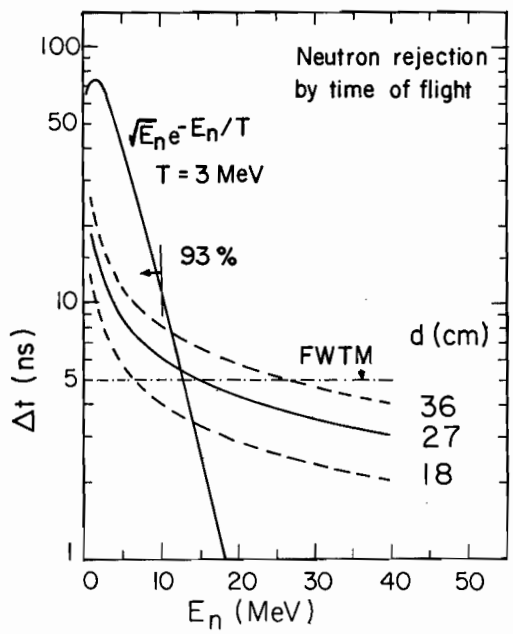

Fig. 12. TOF as a function of neutron energy for the indicated flight paths corresponding to the front, mid-point, and back of each NaI detector. An evaporation spectrum with a 3 MeV temperature is also shown. The 93% limit is shown by the vertical line.

Superimposed is shown a neutron spectrum corresponding to a temperature of 3 MeV. The horizontal line corresponds to 5 ns. With the typical timing resolution of 4.5 ns FWTM [Fig. 5] identification of all pulses from neutrons with $E_n \leq 7$, 17, or 30 MeV for the front, middle, and back of the detectors can be made by their time-of-flight. This ensures that ∿95% of the neutrons can be thus identified. Fig. 13 shows a density map of the TOF spectrum from a PuBe source measured with one of the detectors at the normal front distance of 17.8

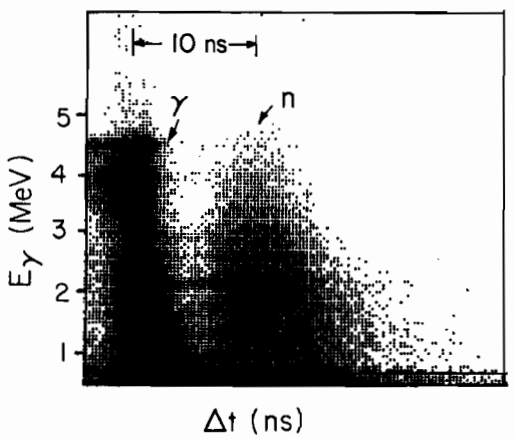

Fig. 13. Density map of a TOF spectrum from a PuBe source at distance of 17.8 cm recorded with one of the NaI detectors. The start was provided by any γ-ray striking an NE-213 scintillator in which neutron pulses were rejected by pulse shape discrimination.

cm from the source. The γ-ray pulses in an NE-213 scintillator were used to provide the start. The 4.43 MeV γ-rays from ^{12}C are clearly seen. Complete identification of the ∿4.7 MeV neutrons is also visible.

It should be mentioned here that significant probability exists for coincidence summing between γ-rays and neutrons. In this case the TOF information will indicate that the event is a γ-ray, while the associated pulse height would be the sum from the γ-ray and the neutron. Such responses to individual detectors can be identified from their pulse shape information. Corrections to the pulse height can then be applied.

6. THE FIRST FEW EXPERIMENTS WITH THE SPIN SPECTROMETER

At present a number of necessary tests are being made to establish the proper performance of the instrument. These include measurements of the background radiation on site with and without beam through the apparatus, counting rate stability with the beam on target, and response to neutrons from heavy-ion reactions. In parallel, calibrations of the entire spectrometer for the determination of the response to single and to multiple γ-rays are being made. Below we describe the essential features of the first few experiments that will be carried out by several groups.

A) Population of Entry States in Fusion Reactions

At first we plan to use a Ge(Li) detector operated in coincidence with the spectrometer using previously investigated reaction systems. By analyzing the Ge(Li) spectra as a function of (H,k) the population of the entry states to various (HI,xn) channels will be determined. The detailed feeding patterns into the ground bands and several side bands in collective and non-collective nuclei will be examined under suitable (H,k) selection. We hope to learn to what extent one can select nuclei populated in different regions of the (E^*,J) space and how the intensities of the observable discrete transitions vary with E^* and J.

From the same measurements we plan to use the high detection efficiency of the apparatus to explore the multipole character of the continuum radiation by selecting aligned nuclear states taking advantage of the angular correlation enhancement from multiple coincidences in pre-

selected NaI detector planes.

We plan to investigate the number of yrast and statistical γ-rays as a function of selected excitation energy and angular momentum. This can be done using external large NaI detectors operated in coincidence with the Spin Spectrometer. However, use of the spectral information of the detectors in the spectrometer will be made to extract the same information with very good statistics. The large efficiency under these conditions will permit us to select exit channels in addition to regions in the (E^*,J) space.

B) Moments-of-inertia at high spin

Knowledge of the moment-of-inertia is important for the understanding of nuclear deformation, loss of pairing correlation, and the single particle contribution in creating the angular momentum states for high spins.

There are two methods that will be used to obtain the effective moment-of-inertia as a function of spin.

The first one involves recording and unfolding the spectrum of the γ-continuum with a large NaI detector external to the spectrometer as a function of (H,k). Comparisons of the structure of the quadrupole bump from progressively higher initial spin states (suitable H,k choice) will permit one to deduce the effective moment-of-inertia as a function of spin.

The second approach involves the proper unfolding of spectra from the detectors in the spectrometer. This method provides ∿500 times more statistics compared to that with an external detector. This will make for selection of exit channels with the Ge(Li) detector possible, in addition to the (H,k) selection. This method will provide data at the Ge(Li) singles rate.

In addition, the collective moment-of-inertia associated with intra-band cascades that de-excite the same entry states can also be measured employing the E_γ-E_γ correlation technique [5]. The significant advantages of carrying our such measurements with the Spin Spectrometer is to sort the data according to (H,k) and thus control the length of the γ-cascades to be studied. Selection of the exit channel by a Ge(Li) detector in this type of measurement appears also possible. Finally, triple correlations E_γ-E_γ-E_γ will be investigated to learn more about the nature and number of transitions within the collective bands.

C) Particle emission as probe of fusion-like reactions

The first experiments will employ equilibrium fusion and will involve detection of light charged particles in coincidence with evaporation residues observed with particle counters. We plan (a) to investigate the effect of angular-momentum and total γ-energy selection on the energy spectra and the angular correlations of the emitted charged particles. The particle correlations can provide effective moments of inertia (spin cut-off factors) at high excitation and spin; (b) to determine the entry state population following α-particle evaporation; (c) to determine for comparison with (a) the moments-of-inertia during γ-decay from unfolding of associated γ-ray spectra of NaI detectors in the spectrometer.

We further plan to select from the same measurements aligned nuclei populated in narrow J distributions. This is accomplished by utilizing the stretched quadrupole nature of the emitted γ-radiation and requiring a high order coincidence with up to 14 NaI detectors in a plane. The nuclear spins are thus selected to be aligned perpendicular to the beam-containing a ring of NaI detectors. Simultaneous selection of (H,k) can

be made to select only narrow ranges of J values. ...w, when α-particles associated with evaporation residues are detected in-plane with a ring of NaI counters their angular correlation becomes isotopic. In contrast, the out-of-plane α-correlations become more anisotropic [6].

The high efficiency of the Spin Spectrometer can provide, for example, good alignment of spins in the range 60 ± 7 ħ. Under such conditions the angular correlations, the particle energies [7] and the particle yields [8] may be sensitive to the shape of the emitting system [9]. This may provide a new method for exploring the shapes of nuclei with high angular momenta. These possibilities will be explored in detail.

D) Incomplete fusion reactions

Recently it has been shown that incomplete fusion [10] of 152 MeV ^{16}O with ^{154}Sm is associat...l with peripheral collisions. These processes also appear to occur [11] only in a narrow band of ∿7 ħ units in the entrance channel. Such processes, highly localized in ℓ, should lead to drastically different populations of entry states following particle emission, when compared to equilibium complete fusion. A careful mapping of the entry states following incomplete fusion reactions as a function of type, angle and energy of the forward emitted charged particles will provide the necessary data for a detailed understanding of the factors governing the onset of these processes.

In addition, using stretched-quadrupole correlation alignment techniques, we hope to determine the degree of spin alignment introduced in incomplete fusion. If significant alignment is intro...iced by this process itself, then combining it with the correlation alignment mentioned earlier may turn out to be a better approach in answering the question about nuclear shapes at very high excitation and spin.

E) Non-equilibrium neutrons from fusion reactions

Various models have been proposed to account for fast forward neutrons observed [12] in heavy-ion fusion reactions. For example, incomplete fusion is highly peripheral, while PEP emission [13] (Fermi jets) is expected to be more central and cover a broader range of lower angular momenta. Conventional multiplicity arrangments cannot easily provide the associated γ-ray multiplicity [12] with the fast component of neutrons because of limited statistics. With the use of the Spin Spectrometer measurements of the γ-ray multiplicity associated with emission of neutrons of various energies and angles should be easier. Such results should provide a basis for selecting among the models and should stimulate theoretical work on the angular momentum dependence.

In addition to the multiplicity information, use of the Spin Spectrometer would provide valuable data on the excitation energies of the entry states following non-equilibium emission of neutrons.

F) Role of angular momentum in deeply inelastic collisions

Measurements of these multiplicity and energy distributions of γ-rays emitted following deeply inelastic collisions (DIC) yield information on a number of questions about the mechanism of DIC. Among these are: (a) What is the role of tangential friction and what types of tangential motion are important in DIC? (b) What partial waves in the entrance channel are involved in DIC and how do they compete with fusion-like processes? (c) What is the connection between the widths of the γ-ray multiplicity distributions or the out-of-plane angular correlation of γ-rays and the degree of alignment of the transferred angular momenta [14]?

(d) What are the differences or similarities of the population of entry states following DIC and fusion-like reactions? Are the products formed at all the available J-values or are only low J values populated? (e) What is the degree of spin alignment in the final fragments? (f) Is it possible to determine separately the number and characteristics of the γ-rays from the target-like and projectile-like fragments?

Such questions will be addressed first with simple measurments involving a few heavy-ion ΔExE telescopes operated in coincidence with the Spin Spectrometer. Future experiments will incorporate simultaneous detection of emitted light charged particles and neutrons.

The excellent cooperation of the personnel at the Washington University Cyclotron Machine Shop is appreciated.

REFERENCES

*Work supported in part by the U.S. Department of Energy under contract No. EY-76-S-02-4052.

**Operated for the U.S. Department of Energy by Union Carbide Corporation under contract No. W-7405-eng-26.

1) D.G. Sarantites, R. Lovett, and R. Woodward, Nucl. Instr. Meth. (in press).

2) Harshaw Chemical Co., Solon, Ohio.

3) A larger version of the device described by D.C. Hensley IEEE Transactions on Nuclear Science, Vol. NS-26, No. 4, p. 4454 (1979).

4) Defined as the states populated following particle emission.

5) O. Andersen, J.D. Garrett, G.B. Hagemann, D. L. Hillis, and L.L. Riedinger, Phys. Rev. Lett. 43, 687 (1979).

6) L. Adler, J.B. Natowitz, M.N. Namboodiri, H. Ho, S. Simon, P.L. Gontheir, A. Khodai and R. Terry, Bull. Am. Phys. Soc. 24, 834 (1979) EB-9.

7) V.A. Karnaukhof, Nucl. Phys. A294, 246 (1978).

8) M. Blann, Phys. Lett. 88B, 5 (1979).

9) S. Cohen, F. Plasil and W.J. Swiatecki, Ann. Phys. 82, 557 (1974).

10) K.A. Geoffroy, D.G. Sarantites, M.L. Halbe[illegible] D.C. Hensley, R.A. Dayras, and J.H. Barke[illegible] Phys. Rev. Lett. 43, 1303 (1979).

11) J.H. Barker, J.R. Beene, M.L. Halbert, D.C. Hensley, M. Jääskeläinen, D.G. Sarantites and R. Woodward (to be published).

12) L. Westerberg, D.G. Sarantites, D.C. Hensley, R.A. Dayras, M.L. Halbert, and J.H. Barker, Phys. Rev. 18, 796 (1978); K.A. Geoffroy et al., (to be published).

13) J.P. Bondorf, J.N. De, G. Fái, A.O.T. Karvinen, B. Jakobsson and J. Randrup, Nucl. Phys. A333, 285 (1980).

14) R.A. Dayras, R.G. Stokstad, C.B. Fulmer, D.C. Hensely, M.L. Halbert, R.L. Robinson, A.H. Snell, D.G. Sarantites, L. Westerberg, and J. H. Barker, Phys. Rev. Lett. 42, 697 (1979).